Zhao *et al. Chem. Synth.* **2025**, *5*, 63
DOI: 10.20517/cs.2024.180

Chemical Synthesis

Research Article

Open Access

Check for updates

Efficient photocatalytic methane conversion to oxygenates over TiO_2 and Pd co-modified titanium silicalite zeolite

En-Dian Zhao[1,2,#], Yihong Chen[1,2,#], Junchi Xu[1], Jun Ma[1,2,*], Dong Liu[1,2,*], Yujie Xiong[1,2,*]

[1]School of Chemistry and Materials Science, University of Science and Technology of China, Hefei 230026, Anhui, China.
[2]Sustainable Energy and Environmental Materials Innovation Center, Nano Science and Technology Institute, Suzhou Institute for Advanced Research, University of Science and Technology of China, Suzhou 215123, Jiangsu, China.
[#]The authors contributed equally to this work.

[*]**Correspondence to:** Prof. Yujie Xiong, Prof. Dong Liu and Dr. Jun Ma, School of Chemistry and Materials Science, University of Science and Technology of China, No.96, Jinzhai Road, Hefei 230026, Anhui, China. E-mails: yjxiong@ustc.edu.cn; dongliu@ustc.edu.cn; junma12@ ustc.edu.cn

How to cite this article: Zhao, E. D.; Chen, Y.; Xu, J.; Ma, J.; Liu, D.; Xiong, Y. Efficient photocatalytic methane conversion to oxygenates over TiO_2 and Pd co-modified titanium silicalite zeolite. *Chem. Synth.* **2025**, *5*, 63. https://dx.doi.org/10.20517/cs.2024.180

Received: 16 Nov 2024 **First Decision:** 26 Dec 2024 **Revised:** 9 Jan 2025 **Accepted:** 8 Feb 2025 **Published:** 15 Jul 2025

Academic Editor: Feng Shi **Copy Editor:** Shu-Yuan Duan **Production Editor:** Shu-Yuan Duan

Abstract

As a type of significant porous material, molecular sieves possess substantial application potential, particularly for catalysis and sustainability. However, the utilization of molecular sieves for photocatalytic synthesis has been hampered by the low charge transfer and poor photoresponse. Herein, we demonstrate that titanium silicalite (TS) zeolite serves as a versatile support integrated with TiO_2 and Pd for selective photocatalytic methane conversion into oxygenates. Comprehensive characterizations indicate that the pore structures of TS zeolite can enhance the adsorption and the localized concentration of reactants for subsequent reactions, while the Pd cocatalyst functions as the photogenerated hole acceptors under light illumination, forming $Pd^{\delta+}$ species to facilitate the C-H bond cleavage of CH_4 molecules. As a result, the optimal Pd-TS@TiO_2 catalyst achieves a high production rate of 6.8 mmol g^{-1} h^{-1} with a selectivity of 96.5% for oxygenate products. This work provides valuable insights into reaction regulation through material design and paves the way for efficient methane conversion to high-value oxygenates.

Keywords: Methane conversion, photocatalysis, artificial photosynthesis, titanium silicalite zeolite, reactive oxygen species, oxygenate production

INTRODUCTION

With the emerging exploration of large reserves of shale gas, coalbed methane, and methane hydrate, methane (CH_4) has received increasing attention as a feedstock for valuable chemicals and fuels[1,2]. Currently, less than 10% of global methane production is used for chemical manufacturing, primarily due to the stubborn C-H bonds and negligible polarizability of methane molecules. Traditional indirect technologies for methane conversion, such as dry reforming of methane, generally require harsh conditions to activate the inert C-H bonds of methane molecules, resulting in high energy costs[3-6]. Therefore, the direct catalytic activation of methane for the synthesis of valuable chemicals and fuels under mild conditions is significant for the sustainable utilization of methane[7-12].

Specifically, the emerging photocatalytic partial oxidation of CH_4 can efficiently transform methane to synthesize value-added oxygenate compounds under mild conditions even at room temperature[13]. This process occurs due to the action of the photogenerated reactive oxygen species, such as hydroxyl radicals (·OH) and superoxide radicals, which efficiently cleave the C-H bonds of methane[14-16]. For instance, Ye *et al.* demonstrated cocatalyst (Pt, Pd, Au, or Ag) loaded ZnO photocatalyst for selective oxidation of CH_4 using only O_2 to synthesize liquid oxygenates[17]. Despite these advances, the deep dehydrogenation or excessive oxidation of methane molecules still hampers the practical application of photocatalytic methane technology[2,18-20]. In this context, it is highly desirable to simultaneously regulate the adsorption configuration of the intermediates and the reaction microenvironment in the photocatalytic methane conversion system to improve the selectivity of target products. Molecular sieves (e.g., Zeolites) possess regular pore channel structures and large specific surface areas, enabling the formation of multi-dimensional reaction site structures[21]. Thus, this approach presents a promising avenue for photocatalytic methane conversion by integrating metal sites with molecular sieves, facilitating an adequate reaction microenvironment to simultaneously regulate the activation processes of CH_4 and oxygen species[22-24].

Here, we present the combination of titanium silicalite (TS) zeolite support with TiO_2 and Pd (Pd-TS@TiO_2) to achieve efficient photocatalytic methane conversion using oxygen as the oxidant. Comprehensive characterizations demonstrated that the pores of TS could significantly enhance the adsorption of reactants for photocatalytic reactions. Pd could accept photogenerated holes to form oxidized $Pd^{\delta+}$, which greatly facilitates the polarization of CH_4 molecules for further activation. Moreover, the methyl radicals (·CH_3) and ·OH species are the key intermediates for CH_4 conversion in the presence of O_2 and H_2O. As a result, the optimized Pd-TS@TiO_2 catalyst achieved a total oxygenate yield of 6.8 mmol g^{-1} h^{-1} with a selectivity of 96.5%.

EXPERIMENTAL

Preparation of TS@TiO_2

The TS molecular sieve TS-1 was purchased from Jiangsu Xianfeng Nano Material Technology Co., Ltd. (XFF08). Firstly, 0.936 g of TS powder was dispersed into 30 mL of ethanol under ultrasonic. Then, 0.4 mL of tetra-n-butyl titanate (TBOT) and 300 μL of H_2O were dropwise added into the above mixture. After stirring for 4 h, the mixture was transferred into a Teflon-lined autoclave and reacted at 180 °C for 3 h. After that, the white powder was collected through a centrifuge, washed three times using ethanol, and dried in an oven. The sample was then annealed at 550 °C for three hours, denoted as TS@TiO_2. The composite samples with different TiO_2 ratios were synthesized by varying the amount of TBOT.

Loading of metal nanoparticles

The Pd nanoparticles were loaded by the photodeposition method or hydrogen reduction method. Typically, 200 mg of the TS@TiO_2 sample was dispersed in 30 mL of water under stirring. Subsequently, 200

uL of K_2PdCl_6 aqueous solution with a concentration of 3.08 mg mL^{-1} was added into the solution and then purged with argon for 30 minutes to remove oxygen. After stirring for another ten hours, the solution was irradiated under a light intensity of 100 mW cm^{-2} for 30 min. After the photodeposition, the sample was collected by centrifugation, washed three times with water, and dried in a vacuum oven. The obtained samples can be denoted as 0.2Pd-TS@TiO.

Photochemical CH_4 conversion measurement

The customized high-pressure stainless-steel reactor is used to test the photocatalytic methane conversion. Firstly, 10 mg of the catalyst was dispersed in 120 mL of ultrapure water and then transferred into the pressurized stainless steel reactor. After finely sealed, the suspension was pursed with ultra-pure oxygen (99.999%) three times to completely remove the air. Then, 1 bar O_2 was maintained in the reactor. Methane (99.999 vol.%) was next injected to acquire the desired pressure. The photocatalytic methane conversion was conducted under ultraviolet light of 365 nm for 2 h. After the reaction, the gaseous products were measured by the gas chromatograph. The CH_3OH and CH_3OOH were analyzed by the 400 MHz liquid superconducting nuclear magnetic resonance spectrometer, while the HCHO was measured through the colorimetric method on the ultraviolet-visible (UV-Vis) spectrophotometer.

RESULTS AND DISCUSSION

The TS zeolite was selected as the support because the presence of titanium ions and the unique -Ti-O-Ti- structure in the TS framework can effectively promote C-H bond activation of methane molecule and the well-defined microporous structure of TS benefits molecule diffusion for further catalytic reaction[21,25,26]. The commercial TS molecular sieve exhibits an ellipsoidal morphology with a particle size of about 300 nm. Subsequently, the TiO_2 was introduced through solvothermal method to prepare TiO_2-TS composite (TS@TiO_2). As shown in Supplementary Figures 1 and 2, scanning electron microscopy (SEM) and transmission electron microscopy (TEM) characterizations revealed the presence of TiO_2 nanoparticles with an approximate size of 10 nm on the TS surface. Furthermore, the amount of TiO_2 nanoparticles on the surface increases with the amount of the added titanium precursor [Supplementary Figure 2]. Subsequently, the Pd cocatalyst was further loaded on the TS@TiO_2 sample by photodeposition (Pd-TS@TiO_2). As a result, the uniform distribution of Pd particles with a size of ~ 2.5 nm was observed on the surface of TS@TiO_2 [Figure 1A and B], while the structure of TS@TiO_2 was well maintained. The high-resolution TEM (HRTEM), high-angle annular dark-field scanning transmission electron microscope (HAADF-STEM), and energy-dispersive X-ray spectroscopy (EDS) mapping analysis [Figure 1C and D] further demonstrated the modifications of TiO_2 and Pd on the surface. Moreover, the distinct lattice fringe spacing of 0.22 nm is assigned to the (111) plane of Pd. The Pd particles observed in the HRTEM analysis indicate a uniform distribution with an average size of 1.9 nm [Supplementary Figure 3].

The N_2-sorption isotherm for the Pd-TS@TiO_2 sample [Supplementary Figure 4] exhibits similar adsorption-desorption isotherms as those of TS and TS@TiO_2. All samples have mesopore volume distribution [Figure 1E and Supplementary Table 1]. These results suggest that the loading of Pd did not alter the original pore size and pore volume of TS, thereby ensuring the diffusion of reactants under liquid-phase reaction conditions. The X-ray diffraction (XRD) patterns of TS were well preserved upon the loading of Pd and TiO_2 [Figure 1F, and Supplementary Figures 5A and 6A]. At high loading amounts of TiO_2 particles, the characteristic patterns attributed to TiO_2 became obvious, while the absence of metallic Pd patterns may be ascribed to the low loading amount of only 0.2% [Supplementary Figure 7] as detected by inductively coupled plasma atomic emission spectroscopy (ICP-OES). The UV-Vis diffuse reflectance spectra [Supplementary Figures 5B, 6B, and 8] show that the pristine TS exhibits two distinct absorption edges. The absorption edge at the wavelength of 218 nm can be attributed to the transition absorption of

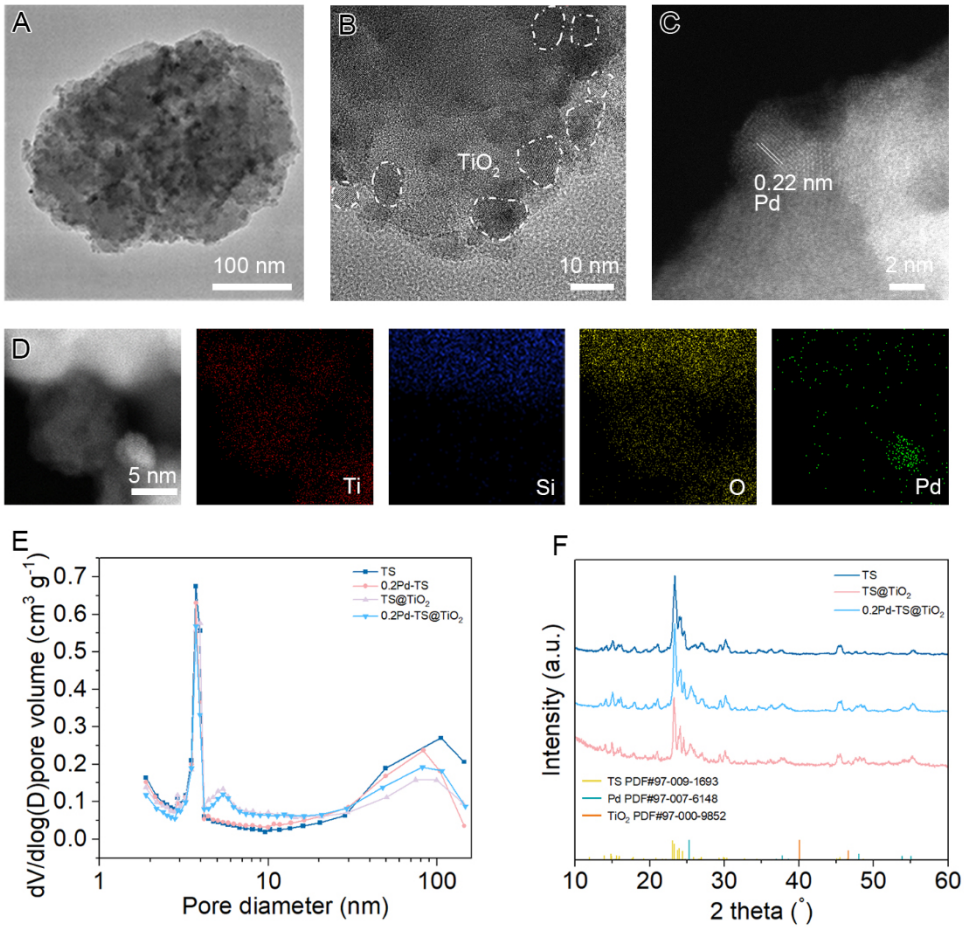

Figure 1. (A) TEM; (B) HRTEM; (C) HAADF-STEM; and (D) elemental mapping images of 0.2Pd-TS@TiO_2; (E) Pore size distribution plots of TS, 0.2Pd-TS, TS@TiO_2, and 0.2Pd-TS@TiO_2 samples derived from N_2-sorption isotherms; (F) The XRD patterns of TiO_2, TS, TS@TiO_2, and 0.2Pd-TS@TiO_2 samples. TEM: Transmission electron microscopy; HRTEM: high-resolution TEM; HAADF-STEM: high-angle annular dark-field scanning transmission electron microscope; TS: titanium silicalite.

tetracoordinated titanium in the TS framework[27]. In contrast, the absorption edge at the wavelength of 330 nm is similar to the transition absorption of hexacoordinated titanium in titanium oxide. It is noteworthy that the loading of Pd and TiO_2 on the TS surface can significantly enhance the light absorption ability of TS, which would improve the performance of photocatalytic reactions. Ultraviolet photoelectron spectroscopy (UPS) was further employed to characterize the energy band structure of the 0.2Pd-TS@TiO_2 sample [Supplementary Figure 9]. Combined with the UV-vis diffuse reflectance spectrum, the band structure of 0.2Pd-TS@TiO_2 can be schematically illustrated in Supplementary Figure 10.

The X-ray photoelectron spectroscopy (XPS) was conducted to analyze the valence states. The TS, Pd@TS, TS@TiO_2, and 0.2Pd-TS samples mainly show the intrinsic signals of Ti, Si, and O inherent to the TS zeolite. The high-resolution Ti 2p XPS spectra [Figure 2A] show the characteristic peaks at 464.3 and 458.5 eV corresponding to Ti^{4+}. The characteristic peaks at 457.5 and 462.5 eV correspond to Ti^{3+}. The Si 2p XPS spectra [Figure 2B] show a characteristic signal for TS zeolite (102.5 eV and 103.5 eV). In addition, the high-resolution O 1s XPS spectra [Figure 2C] for the peak at 529.8 eV correspond to TiO_2, while the peak at 532.5 eV corresponds to oxygen from TS[26]. Interestingly, the signal attributed to oxygen vacancy can be observed at 531 eV upon Pd loading[28]. Meanwhile, the Pd 3d XPS spectra mainly show the distinctive peaks for

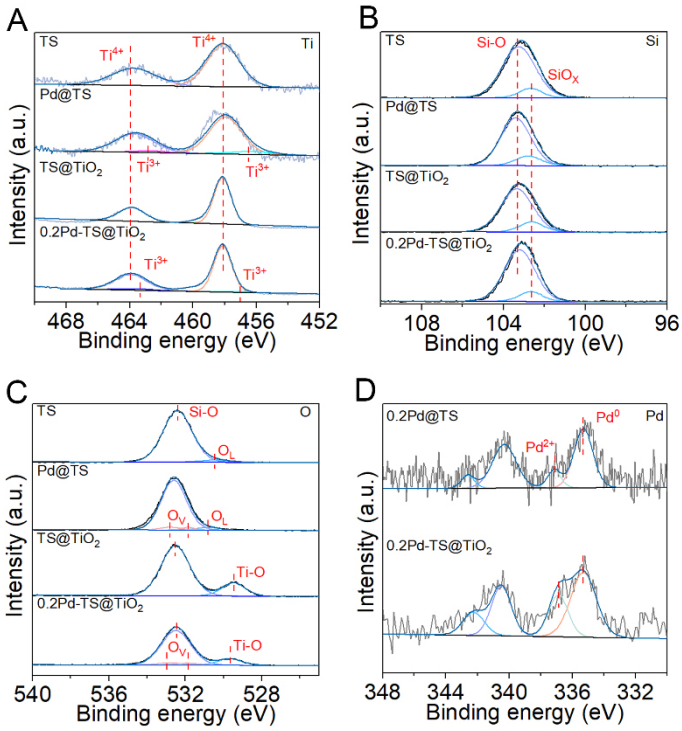

Figure 2. (A)Ti 2p; (B) Si 2p; (C) O 1d and (D) Pd 3d XPS spectra of TS, $TS@TiO_2$, 0.2Pd-TS and $0.2Pd\text{-}TS@TiO_2$. XPS: X-ray photoelectron spectroscopy; TS: titanium silicalite.

metallic Pd [Figure 2D]; oxidized Pd species can also be observed. These results indicate the interaction between Pd and the support. Notably, the loading of TiO_2 would increase the ratio of oxidized Pd and enhance the interaction between Pd and the support.

Upon recognizing the structure of $Pd\text{-}TS@TiO_2$, the photocatalytic methane conversion performance was then evaluated over $Pd\text{-}TS@TiO_2$ and control samples using oxygen as the oxidant in an aqueous-phase catalytic system. As shown in Figure 3A, both the pristine TS and TiO_2 can drive methane conversion to generate CH_3OH, CH_3OOH, HCHO, and a small amount of CO_2 with a total production rate of 1.4 and 1.5 mmol g^{-1} h^{-1}, respectively. The performance of methane conversion over TS would be slightly improved upon the introduction of TiO_2 or Pd on the surface. It was unexpected that the performance for methane conversion over $0.2Pd\text{-}TS@TiO_2$ would be greatly enhanced, with a production rate of 6.8 mmol g^{-1} h^{-1} and a selectivity of 96.5% for oxygenate products. The enhanced performance is mainly beneficial from the unique pore structure of the TS support and the synergetic effect of TiO_2 and Pd. Interestingly, the photocatalytic methane conversion performance over the physical mixing of TS, TiO_2, and Pd ($0.2Pd\text{-}TS + TiO_2$) is much lower than that of the $0.2Pd\text{-}TS@TiO_2$ sample [Figure 3B]. The different metal-modified $TS@TiO_2$ catalysts exhibit inferior activities on photocatalytic methane conversion $Pd\text{-}TS@TiO_2$ catalyst [Supplementary Figures 11-14]. These results further confirm that the intimate combination and synergistic effect among TS, TiO_2, and Pd play an essential role in photocatalytic methane conversion. In addition, a series of control experiments suggest that catalyst, light, and CH_4 are critical factors in the photocatalytic CH_4 conversion over $Pd\text{-}TS@TiO_2$ [Supplementary Figure 15]. Subsequently, the test was performed by varying the loading amount of metallic Pd to screen the optimal photocatalyst sample on its methane conversion performance. As shown in Figure 3C, the photocatalytic performance over the $Pd\text{-}TS@TiO_2$ sample showed a classic volcano-shaped distribution trend with the Pd loading amount, among which the $0.2Pd\text{-}TS@TiO_2$ reached the highest production rate for oxygenate compounds.

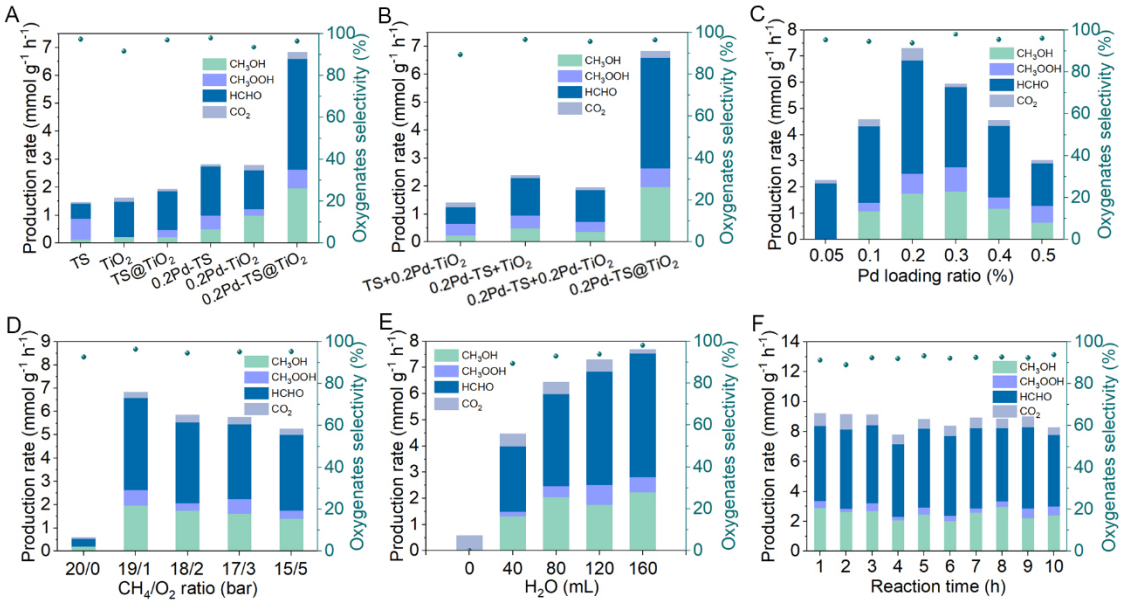

Figure 3. (A) Photocatalytic methane conversion performance of Pd-TS@TiO_2 and the control samples; (B) Comparison of photocatalytic methane conversion performance with physical mixed samples; (C) Photocatalytic methane conversion performance of Pd-TS@TiO_2 samples with different metal loadings; Photocatalytic methane conversion performance of the 0.2Pd-TS@TiO_2 sample under (D) different CH_4/O_2 ratios and (E) different amounts of H_2O; (F) Cyclic tests of 0.2Pd-TS@TiO_2 catalyst. TS: Titanium silicalite.

After identifying the optimal catalyst, an evaluation was conducted to ascertain the influence of experimental parameters on photocatalytic methane conversion. Firstly, the molar ratio of CH_4 to O_2 was examined over the optimized 0.2Pd-TS@TiO_2 with a total 20 bar pressure. As revealed in Figure 3D, a much lower yield of oxygenates (0.54 mmol g^{-1} h^{-1}) was obtained under anaerobic conditions, manifesting the essential role of O_2 in CH_4 activation. In sharp contrast, the production rate of oxygenates was markedly enhanced, reaching 6.8 mmol g^{-1} h^{-1} at CH_4/O_2 = 19/1. Nevertheless, the yield of oxygenates would gradually decrease at a lower CH_4/O_2 ratio, which can be ascribed to the decreased CH_4 concentration in water under decreased CH_4 pressure. Thereafter, photocatalytic CH_4 conversion tests with varying amounts of water were carried out to explore the effect of water on CH_4 oxidation. As a result, photocatalytic CH_4 conversion in the gas-solid phase without adding water brings out only CO_2 as a by-product due to the severe oxidation of CH_4 [Figure 3E]. As the amount of water and dissolved methane increased, both the production rate and selectivity of liquid oxygenates gradually increased, since water could promote oxygenate desorption from the surface of the catalyst and alleviate the overoxidation. Additionally, all of the products gradually increase with the reaction [Supplementary Figure 16], suggesting that the catalytic reaction was effective and continuous under the described conditions.

In order to investigate the role of titanium-silicon molecular sieve (TS) in the photocatalytic conversion of methane, we carried out a series of control experiments. Initially, the porous structure of TS was disrupted by ball milling (Pd-TS@TiO_2-BM). As shown in Supplementary Figure 17, the Pd-TS@TiO_2-BM exhibits diminished performance for photocatalytic methane conversion. Alkaline treatment was employed to etch the pristine TS zeolite to destroy the TS pores (NaOH-TS). The resulting composite catalyst was then decorated with Pd and TiO_2 (0.2Pd-NaOH-TS@TiO_2)[29]. We also replaced the TS with silica spheres (SiO_2) [Supplementary Figure 18] without pores to prepare the composite catalyst (Pd-SiO_2@TiO_2). As an outcome, the performance of photocatalytic CH_4 conversion over both 0.2Pd-SiO_2@TiO_2 and 0.2Pd-NaOH-SiO_2@TiO_2 is significantly lower than that over the 0.2Pd-TS@TiO_2 sample [Supplementary Figure 19].

These results firmly suggest that the pore of TS zeolite plays a crucial role in photocatalytic methane conversion, which may concentrate methane molecules, thereby increasing the local concentration and facilitating the interaction of reactants with active sites. Subsequently, the stability of the Pd-TS@TiO_2 catalyst was then examined. As shown in Figure 3F, both the production and selectivity of the oxygenates generated from CH_4 conversion were well maintained over ten consecutive cycles. In addition, both morphology and crystal phase show negligible changes after the stability test, confirming the excellent catalytic stability of the Pd-TS@TiO_2 catalyst.

Upon recognizing the superior performance of methane conversion by modifying TS with TiO_2 and Pd, we are now able to gain a fundamental insight into the reaction mechanism over Pd-TS@TiO_2. As evidenced by the photoluminescence and photoelectrochemical measurements [Supplementary Figure 20], the modification of TiO_2 and Pd can significantly enhance the separation efficiency of photogenerated charge carriers[30-32]. Additionally, the electrochemical impedance spectroscopy (EIS) measurements were conducted to compare the transport resistance of photogenerated electrons [Supplementary Figure 21]. The 0.2Pd-TS@TiO_2 presents the lowest impedance, indicating efficient electron transport upon Pd and TiO_2 loading. The synergistic effect of both Pd and TiO_2 significantly lowers the electron transport resistance, resulting in superior photocatalytic performance for methane oxidation. Moreover, as observed by in situ XPS under light illumination, the valence state of Pd would gradually change from a metallic state (Pd^0) to an oxidized state ($Pd^{\delta+}$), while the Si, O, and Ti elements exhibit negligible change under light illumination [Supplementary Figure 22][33,34]. These results suggest that Pd can trap photogenerated holes under light illumination, and the oxidized $Pd^{\delta+}$ can facilitate photocatalytic methane conversion towards oxygenates[35].

Given the indispensable role of oxygen species in photocatalytic methane activation, the *in situ* electron paramagnetic resonance (EPR) was conducted to monitor the reactive oxygen species in the process of photocatalytic CH_4 conversion. As shown in Figure 4A, the intensity of the hydroxyl radicals (·OH) exhibits typical quartet signals with an intensity ratio of 1:2:2:1. The signals of TS@TiO_2 and Pd-TS@TiO_2 are much stronger than those of the TS and Pd-TS. This may be attributed to the presence of abundant titanium-oxygen sites upon the introduction of TiO_2, which are conducive to the activation of oxygen to generate ·OH species[36]. Moreover, both the characteristic signals of $\cdot CH_3$ and ·OH can be detected in the EPR spectra [Figure 4B] for Pd-TS@TiO_2 in the CH_4 atmosphere under light irradiation, indicating that the CH_4 molecule could be efficiently activated over Pd-TS@TiO_2 catalyst for further conversion. Then, temperature-programmed desorption (TPD) was employed to investigate the adsorption behaviors of the reactants on the catalyst surface. As illustrated in Figure 4C, the O_2-TPD profile for 0.2Pd-TS@TiO_2 exhibits strong O_2 desorption peaks at about 95 and 300 °C, respectively. In comparison, the O_2-TPD profiles for TS, Pd-TS, and TS@TiO_2 show much weaker O_2 desorption peaks. This observation indicates the enhanced O_2 adsorption upon the co-modification of Pd and TiO_2. Similarly, the CH_4-TPD profile for 0.2Pd-TS@TiO_2 shows much stronger CH_4 desorption peaks (100 and 300 °C) than that for TS, Pd-TS, and TS@TiO_2 [Figure 4D]. Overall, the enhanced O_2 and CH_4 reactant adsorption capability brought by the synergetic effect of Pd, TiO_2, and TS greatly promotes the performance of photocatalytic CH_4 conversion.

Furthermore, in situ diffuse reflectance infrared Fourier-transform spectroscopy (DRIFTS) was carried out to elucidate the reaction mechanism on the Pd-TS@TiO_2 catalyst. As shown in Figure 4E, obvious peaks at 1,301 and 1,540 cm^{-1} can be observed in the DRIFTS spectrum of Pd-TS@TiO_2 in the dark, which can be attributed to the C-H deformation vibration and C-H symmetric deformation vibrational mode of CH_4, respectively[37]. Additionally, the peaks at 3,650, 3,551, and 1,623 cm^{-1} can be attributed to the vibration absorption of H_2O molecules[38]. Upon light irradiation, the vibrational mode of $*CH_3$ deformation at 1,476 cm^{-1} appears, suggesting the rapid dissociation of CH_4 over the surface of Pd-TS@TiO_2, which is consistent

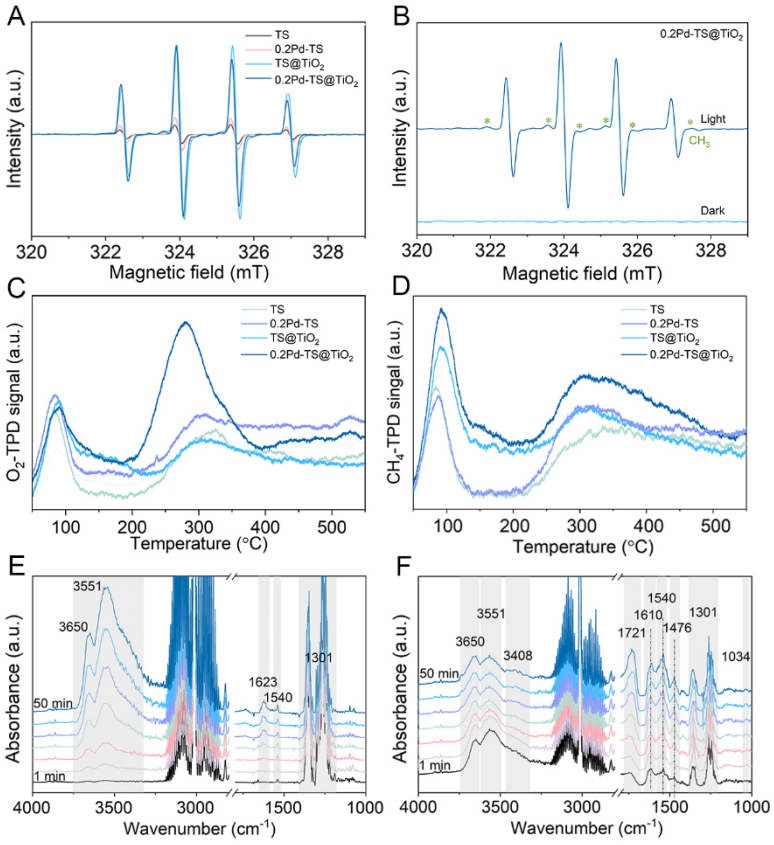

Figure 4. (A and B) EPR spectra of zeolite series samples (TS, TS@TiO_2, 0.2Pd-TS, 0.2Pd -TS@TiO_2) before and after adding light in oxygen-saturated ultrapure water; (C) O_2-TPD and (D) CH_4-TPD profiles of TS, Pd-TS, TS@TiO_2, Pd-TS@TiO_2. *In situ* DRIFTS spectra of 0.2Pd-TS@TiO_2 catalyst (E) in the dark and (F) under light illumination in CH_4 + O_2 + H_2O atmosphere. EPR: Electron paramagnetic resonance; TS: titanium silicalite; TPD: temperature-programmed desorption; DRIFTS: diffuse reflectance infrared Fourier-transform spectroscopy.

with EPR characterizations. Moreover, the peaks of *OH, *OCH_3 and *CH_2O appear and gradually increase at 3,408, 1,034, and 1,721 cm^{-1}, respectively, demonstrating the transformation of the intermediates on the surface under light illumination [Figure 4F][39]. Overall, the DRIFTS results indicate that CH_4 molecules are first activated on the surface of 0.2Pd-TS@TiO_2 to form *CH_3 species, and then undergo the pathway of *OCH_3 and *CH_2O intermediates to further generate oxygenate products (CH_3OH and HCHO). Based on these results, a potential reaction pathway is proposed for photocatalytic methane conversion over 0.2Pd-TS@TiO_2 [Supplementary Figure 23]. In detail, the 0.2Pd-TS@TiO_2 sample is excited under light irradiation to generate electron-hole pairs. The photogenerated holes are enriched on Pd to form $Pd^{\delta+}$ species, while the photogenerated electrons can drive the activation of oxygen to ·OH species. Subsequently, the adsorbed CH_4 molecules would be polarizing induced by $Pd^{\delta+}$ species (steps 1-3), and further be activated to form *CH_3 species. Then, the formed *CH_3 species can couple with ·OH to generate CH_3OH (steps 4-5, path 2), or undergo a stepwise dehydrogenation and oxygenation process to generate HCHO products (step 8, path 1)[40].

CONCLUSIONS

In summary, an effective strategy for selective photocatalytic methane conversion into oxygenates has been demonstrated using TS zeolite-based composite catalysts. The pore structures of TS zeolite can facilitate an increase in the local concentration of reactants for further reaction. The Pd cocatalysts function as the

photogenerated hole acceptors under light illumination and further boost the C-H bond cleavage of CH_4 molecules, while the presence of TiO_2 can promote the formation of reactive oxygen species. As a result, the optimal Pd-TS@TiO_2 catalyst achieves a production rate of 6.8 mmol g^{-1} h^{-1} with a selectivity of 96.5% for oxygenate products. This study proves that molecular sieves are a powerful carrier in photocatalytic synthesis, which may provide a promising avenue for the rational design of photocatalysts for efficient methane conversion.

DECLARATIONS

Acknowledgement

We thank the USTC Center for Micro- and Nanoscale Research and Fabrication, the Instruments Center for Physical Science, University of Science and Technology of China, and the Physical and Chemical Analysis Center at Suzhou Institute for Advanced Research, University of Science and Technology of China, for their support.

Authors' contributions

Conceptualization, investigation, formal analysis and writing original draft: Zhao, E. D.; Chen, Y.
Formal analysis: Xu, J.
Supervision, writing review, and project administration: Ma, J.; Liu, D.; Xiong, Y.

Availability of data and materials

The data and materials supporting the findings of this study are available within the article and its Supplementary Materials.

Financial support and sponsorship

This work was financially supported by the NSFC (22232003, 22279128, and 22409189) and the Natural Science Foundation of Jiangsu Province (BK20240458).

Conflicts of interest

All authors declared that there are no conflicts of interest.

Ethical approval and consent to participate

Not applicable.

Consent for publication

Not applicable.

REFERENCES

1. Fan, Y.; Zhou, W.; Qiu, X.; et al. Selective photocatalytic oxidation of methane by quantum-sized bismuth vanadate. *Nat. Sustain.* **2021**, *4*, 509-15. DOI
2. Guo, X.; Fang, G.; Li, G.; et al. Direct, nonoxidative conversion of methane to ethylene, aromatics, and hydrogen. *Science* **2014**, *344*, 616-9. DOI
3. Diao, J.; Zhang, T.; Xu, Z.; Guo, G. The atomic-level adjacent NiFe bimetallic catalyst significantly improves the activity and stability for plasma-involved dry reforming reaction of CH_4 and CO_2. *Chem. Eng. J.* **2023**, *467*, 143271. DOI
4. Guene, L. B.; Geng, B.; Pan, R.; et al. Solar-driven photothermal catalytic CO_2 conversion: a review. *Rare. Met.* **2024**, *43*, 2913-39. DOI
5. Palmer, C.; Upham, D. C.; Smart, S.; Gordon, M. J.; Metiu, H.; Mcfarland, E. W. Dry reforming of methane catalysed by molten metal alloys. *Nat. Catal.* **2020**, *3*, 83-9. DOI

6. Li, Y.; Liu, C.; Su, Y.; Zhao, Y.; Qiao, B. Maximized Ir atom utilization via downsizing active sites to single-atom scale for highly stable dry reforming of methane. *Chem. Synth.* **2024**, *4*, 61. DOI
7. Schwach, P.; Pan, X.; Bao, X. Direct conversion of methane to value-added chemicals over heterogeneous catalysts: challenges and prospects. *Chem. Rev.* **2017**, *117*, 8497-520. DOI PubMed
8. Li, X.; Tan, T.; Ji, W.; et al. Remarkably enhanced methane sensing performance at room temperature via constructing a self-assembled mulberry-like ZnO/SnO_2 hierarchical structure. *Energy. Environ. Mater.* **2024**, *7*, e12624. DOI
9. Meng, X.; Cui, X.; Rajan, N. P.; Yu, L.; Deng, D.; Bao, X. Direct methane conversion under mild condition by thermo-, electro-, or photocatalysis. *Chem* **2019**, *5*, 2296-325. DOI
10. Saha, D.; Grappe, H. A.; Chakraborty, A.; Orkoulas, G. Postextraction separation, on-board storage, and catalytic conversion of methane in natural gas: a review. *Chem. Rev.* **2016**, *116*, 11436-99. DOI PubMed
11. Yuliati, L.; Yoshida, H. Photocatalytic conversion of methane. *Chem. Soc. Rev.* **2008**, *37*, 1592-602. DOI PubMed
12. Ma, J.; Mao, K.; Low, J.; et al. Efficient photoelectrochemical conversion of methane into ethylene glycol by WO_3 nanobar arrays. *Angew. Chem. Int. Ed. Engl.* **2021**, *60*, 9357-61. DOI
13. Shen, X.; Wu, D.; Fu, X.; Luo, J. Highly selective conversion of methane to ethanol over $CuFe_2O_4$-carbon nanotube catalysts at low temperature. *Chin. Chem. Lett.* **2022**, *33*, 390-3. DOI
14. Choudhary, T. V.; Choudhary, V. R. Energy-efficient syngas production through catalytic oxy-methane reforming reactions. *Angew. Chem. Int. Ed. Engl.* **2008**, *47*, 1828-47. DOI PubMed
15. Zhou, L.; Martirez, J. M. P.; Finzel, J.; et al. Light-driven methane dry reforming with single atomic site antenna-reactor plasmonic photocatalysts. *Nat. Energy.* **2020**, *5*, 61-70. DOI
16. Wang, P.; Shi, R.; Zhao, Y.; et al. Selective photocatalytic oxidative coupling of methane via regulating methyl intermediates over metal/Zno nanoparticles. *Angew. Chem. Int. Ed. Engl.* **2023**, *62*, e202304301. DOI
17. Song, H.; Meng, X.; Wang, S.; et al. direct and selective photocatalytic oxidation of CH_4 to oxygenates with O_2 on cocatalysts/ZnO at room temperature in water. *J. Am. Chem. Soc.* **2019**, *141*, 20507-15. DOI
18. Iglesias-juez, A.; Beale, A. M.; Maaijen, K.; Weng, T. C.; Glatzel, P.; Weckhuysen, B. M. A combined *in situ* time-resolved UV-Vis, Raman and high-energy resolution X-ray absorption spectroscopy study on the deactivation behavior of Pt and PtSn propane dehydrogenation catalysts under industrial reaction conditions. *J. Catal.* **2010**, *276*, 268-79. DOI
19. Marcinkowski, M. D.; Darby, M. T.; Liu, J.; et al. Pt/Cu single-atom alloys as coke-resistant catalysts for efficient C-H activation. *Nat. Chem.* **2018**, *10*, 325-32. DOI
20. Sushkevich, V. L.; Palagin, D.; Ranocchiari, M.; Van Bokhoven, J. A. Selective anaerobic oxidation of methane enables direct synthesis of methanol. *Science* **2017**, *356*, 523-7. DOI PubMed
21. Liang, J.; Liang, Z.; Zou, R.; Zhao, Y. Heterogeneous catalysis in zeolites, mesoporous silica, and metal-organic frameworks. *Adv. Mater.* **2017**, 29. DOI PubMed
22. Shan, J.; Li, M.; Allard, L. F.; Lee, S.; Flytzani-Stephanopoulos, M. Mild oxidation of methane to methanol or acetic acid on supported isolated rhodium catalysts. *Nature* **2017**, *551*, 605-8. DOI PubMed
23. Shi, Y.; Zhou, Y.; Lou, Y.; Chen, Z.; Xiong, H.; Zhu, Y. Homogeneity of supported single-atom active sites boosting the selective catalytic transformations. *Adv. Sci. (Weinh).* **2022**, *9*, e2201520. DOI PubMed PMC
24. Liu, Z.; Shuai, J.; Xu, W.; Lu, X.; Xia, Q.; Zhou, D. Catalytic synthesis of niacin from 3-methyl-pyridine and 30%H_2O_2 by Cu-based zeolite. *Chem. Synth.* **2024**, *4*, 69. DOI
25. Sun, Y.; Li, G.; Gong, Y.; Sun, Z.; Yao, H.; Zhou, X. Ag and TiO_2 nanoparticles co-modified defective zeolite TS-1 for improved photocatalytic CO_2 reduction. *J. Hazard. Mater.* **2021**, *403*, 124019. DOI
26. Yu, B.; Cheng, L.; Wu, J.; et al. Surface hydroxyl group dominating aerobic oxidation of methane below room temperature. *Energy. Environ. Sci.* **2024**, *17*, 8127-39. DOI
27. Yang, Z.; Yu, Q.; Wang, H.; Ge, Q.; Zhu, X. Ketonization of propionic acid over TS-1 and Ti-Beta zeolites: mechanism and effects of topology and hydrophobicity. *J. Catal.* **2024**, *429*, 115247. DOI
28. Hu, W.; Liu, Y.; Withers, R. L.; et al. Electron-pinned defect-dipoles for high-performance colossal permittivity materials. *Nat. Mater.* **2013**, *12*, 821-6. DOI
29. Ma, R.; Chen, W.; Wang, L.; et al. *N*-Oxyl radicals trapped on zeolite surface accelerate photocatalysis. *ACS. Catal.* **2019**, *9*, 10448-53. DOI
30. Do, J. Y.; Son, N.; Chava, R. K.; et al. Plasmon-induced hot electron amplification and effective charge separation by Au nanoparticles sandwiched between copper titanium phosphate nanosheets and improved carbon dioxide conversion to methane. *ACS. Sustainable. Chem. Eng.* **2020**, *8*, 18646-60. DOI
31. Chava, R. K.; Im, Y.; Kang, M. Internal electric field promoted charge separation *via* bismuth-based ternary heterojunctions with near-infrared light harvesting properties for efficient photoredox reactions. *J. Mater. Chem. A.* **2024**, *12*, 18498-511. DOI
32. Do, J. Y.; Chava, R. K.; Mandari, K. K.; et al. Selective methane production from visible-light-driven photocatalytic carbon dioxide reduction using the surface plasmon resonance effect of superfine silver nanoparticles anchored on lithium titanium dioxide nanocubes (Ag@LixTiO_2). *Appl. Catal-B:. Environ.* **2018**, *237*, 895-910. DOI
33. Do, V. H.; Prabhu, P.; Jose, V.; et al. Pd-PdO nanodomains on amorphous Ru metallene oxide for high-performance multifunctional electrocatalysis. *Adv. Mater.* **2023**, *35*, e2208860. DOI
34. Wang, T.; Li, F.; Huang, H.; et al. Porous Pd-PdO nanotubes for methanol electrooxidation. *Adv. Funct. Mater.* **2020**, *30*, 2000534.

DOI

35. Gong, Z.; Luo, L.; Wang, C.; Tang, J. Photocatalytic methane conversion to C1 oxygenates over palladium and oxygen vacancies co-decorated TiO_2. *Solar. RRL.* **2022**, *6*, 2200335. DOI
36. Jiang, Y.; Zhao, W.; Li, S.; et al. Elevating photooxidation of methane to formaldehyde via TiO_2 crystal phase engineering. *J. Am. Chem. Soc.* **2022**, *144*, 15977-87. DOI
37. Ma, J.; Zhu, C.; Mao, K.; et al. Sustainable methane utilization technology via photocatalytic halogenation with alkali halides. *Nat. Commun.* **2023**, *14*, 1410. DOI PubMed PMC
38. Bergonzi, I.; Mercury, L.; Brubach, J. B.; Roy, P. Gibbs free energy of liquid water derived from infrared measurements. *Phys. Chem. Chem. Phys.* **2014**, *16*, 24830-40. DOI PubMed
39. Zheng, K.; Wu, Y.; Zhu, J.; et al. Room-temperature photooxidation of CH_4 to CH_3OH with nearly 100% selectivity over hetero-ZnO/Fe_2O_3 porous nanosheets. *J. Am. Chem. Soc.* **2022**, *144*, 12357-66. DOI
40. Luo, L.; Gong, Z.; Xu, Y.; et al. Binary Au-Cu reaction sites decorated ZnO for Selective methane oxidation to C1 oxygenates with nearly 100% selectivity at room temperature. *J. Am. Chem. Soc.* **2022**, *144*, 740-50. DOI